

Alma Mater Studiorum Università di Bologna
Archivio istituzionale della ricerca

Experimental identification of the material standard linear solid model parameters by means of dynamical measurements

This is the final peer-reviewed author's accepted manuscript (postprint) of the following publication:

Published Version:

Amadori S., Catania G. (2022). Experimental identification of the material standard linear solid model parameters by means of dynamical measurements. JOURNAL OF VIBRATION AND CONTROL, 28(23-24), 3688-3704 [10.1177/10775463211037151].

Availability:

This version is available at: <https://hdl.handle.net/11585/855343> since: 2022-11-15

Published:

DOI: <http://doi.org/10.1177/10775463211037151>


Terms of use:

Some rights reserved. The terms and conditions for the reuse of this version of the manuscript are specified in the publishing policy. For all terms of use and more information see the publisher's website.

This item was downloaded from IRIS Università di Bologna (<https://cris.unibo.it/>).
When citing, please refer to the published version.

(Article begins on next page)

Experimental identification of the material standard linear solid model parameters by means of dynamical measurements

Journal of Vibration and Control
2021, Vol. 0(0) 1–17
© The Author(s) 2021
Article reuse guidelines:
sagepub.com/journals-permissions
DOI: 10.1177/10775463211037151
journals.sagepub.com/home/jvc


Stefano Amadori¹  and Giuseppe Catania²

Abstract

A procedure for the experimental identification of the material standard linear solid model parameters by means of dynamic mechanical analysis test instrument measurements is presented. Since the standard linear solid material stress–strain functional $D(\omega)$ relationship in the frequency domain formally depends on the standard linear solid material parameters, a procedure able to identify these parameters from test measurement estimates is proposed in this work. Nevertheless, a critical, nonlinear and non-parametric approach is to be followed since the number of the material standard linear solid block components is generally unknown, and the material $D(\omega)$ shows a highly nonlinear dependency on the unknown standard linear solid material parameters. For these reasons, measurement and test model noise is expected to strongly influence the accuracy of the identification results. A multi-step procedure is presented, consisting first in the non-parametric identification of a frequency dependent, two degrees of freedom model instrument frame by means of a polynomial rational function, where polynomial order and parameters, such as polynomial coefficients and pole-residue couples, are optimally identified by means of an algebraic numerical technique and of an iterative stabilization procedure. Another procedure able to identify the material $D(\omega)$ polynomial rational functional relationship in the frequency domain is also proposed, taking into account the dynamic contribution of the instrument frame, of the inertial contribution of the distributed mass of the beam and of the lumped mass of the instrument force measuring system. An effective procedure, able to identify the standard linear solid material model parameters in the time domain from the identified material physical poles, is finally proposed. Some application examples, concerning the identification of the standard linear solid model of a known material and of an unknown composite material, are shown and discussed as well.

Keywords

Material modelling, dynamic measurements, model identification, identification technique, rational frequency domain identification

1. Introduction

The standard linear solid (SLS) material model is commonly used to model the σ stress ε strain relationship in many conventional and unconventional materials in the frequency domain, and it consists of a generalized Kelvin (K) model made up of N K-blocks connected in series (Amadori and Catania, 2016, 2017; Findley et al. 1989). Nevertheless, starting from dynamic mechanical measurements on specimens made of the material under study, the identification of the SLS material model order and parameters is not a trivial task since the material $D(\omega) = 1/E_0 \cdot \hat{\sigma}(\omega)/\hat{\varepsilon}(\omega)$, where $\hat{(\cdot)} = \mathcal{F}(\cdot)$ is the Fourier transform operator and $E_0 = \hat{\sigma}(j\omega = 0)/\hat{\varepsilon}(j\omega = 0)$, has to be first identified in a useful $\Delta = [\omega_{min}, \omega_{max}]$ frequency range. Since the $D(\omega = \omega_s), s = 1..n_f$ dependency on the SLS material model parameters can be analytically defined

in closed form for every ω_s frequency measured value, a set of n_f highly non-linear equations in the model parameter unknowns result (Amadori and Catania, 2016, 2017). Moreover, a non-parametric identification problem results since the N model order is unknown.

The material stress strain functional relationship $D(\omega)$ can be estimated from dynamical measurements of excitation

¹Ciri-Mam, University of Bologna, Bologna, Italy

²DIN-Department of Industrial Engineering, Ciri-Mam, University of Bologna, Bologna, Italy

Received: 11 December 2020; accepted: 15 July 2021

Corresponding author:

Stefano Amadori, Ciri-Mam, University of Bologna, Viale Risorgimento 2, Bologna, BO 40136, Italy.
Email: stefano.amadori4@unibo.it

and displacement on homogeneous specimens made of the material under study, by taking into account a known system model depending on the system known geometry, boundary conditions, material known inertial properties (e.g. density ρ) and unknown $D(\omega)$. Dynamic mechanical analysis (DMA) instruments are an established experimental tool that can be employed for this type of tests, involving homogeneous, uniform beam specimens to be excited in axial and flexural conditions in a broad range of experimental setups (Amadori and Catania, 2017; Ehrenstein et al., 2004; Kostka et al., 2016; Liu et al., 2014; Menard, 2008; Oregui et al., 2016; Read and Dean, 1978; Xu and Gupta et al., 2018).

The mathematical model employed generally relies on beam Euler–Timoshenko assumptions, being generally acceptable with respect to the specimen subsystem modelling approach, but normal boundary conditions are generally taken into account, that is, the dynamic contribution of the instrument frame–fixture and of the mobile measuring subsystem is not fully taken into account in the measuring Δ frequency range under study. The specimen frequency response function (FRF) is estimated from the specimen excitation and response measurements at the different frequency values. Depending on the model adopted to describe the specimen and to the specimen known geometry, the relationship between the specimen FRF estimate and $D(\omega)$ is outlined (ASTM International, 2015a, 2015b; Danley, 2018; Storage et al., 2013; Swaminathan and Shivakumar et al., 2009), so that $D(\omega)$ can be identified.

Nevertheless, $D(\omega)$ estimate may highly suffer from the simplified assumed model boundary conditions since the contribution of the system frame–fixture to the measured beam FRF may outline poles that are not simply related to beam geometry and material $D(\omega)$. When beam specimens in various experimental clamping setups are tested, the real experimental boundary conditions should be made as close as possible to the boundary conditions assumed in the adopted system model (Menard, 2008; Storage et al., 2013), but in a practical context the assumed theoretical boundary conditions are generally very different from real boundary conditions, and the contribution of such a difference must be taken into account.

A solution adopted in many known commercial applications is to estimate the static elastic stiffness modelling the ideal coupling between a rigid frame and the specimen and to also estimate the lumped mass associated to the mobile measuring subsystem by means of a calibration procedure. This approach generally results in a simple lumped parameter frame model approach; nevertheless, such an approach generally leads to non-consistent and unsatisfying results (McAninch et al., 2015; Schalnat et al., 2020; Storage et al., 2013) because such simple models do not accurately describe the specimen dynamic behaviour in the medium and high measurement frequency range (Placet and Foltete, 2010; Schalnat et al., 2020).

To increase the results accuracy, more effective calibration techniques involving the identification of the dynamic model of the frame–fixture subsystem are required. Many effective experimental model identification techniques, operating in the time and frequency domain, are known in order to obtain an accurate instrument frame structural model to be coupled with the specimen model and to define a procedure for filtering the estimated specimen FRF from the frame coupling real experimental boundary conditions (Ewins, 2000; Giuliani et al., 2013; Huynh et al., 2021; Peumans et al., 2019; Stanbridge and Ewins, 1999). Nevertheless, such approaches typically require that a high number of experimental dofs are taken into account, being they not directly available from within the typical DMA instrument setup, since only one experimental dof is here available (Amadori and Catania, 2017; Placet and Foltete, 2010; Read and Dean, 1978). An additional multi-channel test system must be employed, and laser doppler vibrometer sensors, accelerometers, impulse and shaker excitation sensors should be employed as well to follow a consistent model frame identification approach (Huynh et al., 2020, 2021; Warren et al., 2011). It must be outlined that while the accuracy of the system calibration can significantly be improved by adopting a multi-dof experimental identification technique, the application of such procedure, to be adopted before any new measurement campaign since the fixturing subsystem varies with respect to any different beam specimen, can be not useful from an engineering point of view because of test time and cost limitations. A multi-dof frame model identification technique requiring only the standard DMA measurement FRF estimates was recently proposed by these authors (Amadori and Catania, 2021). Such approach is based on a beam spectral-modal approach and on the adoption of optimization-based numerical techniques to identify the frame–fixture model subsystem. Nevertheless, the resulting identified model can be not consistent at all in some cases because the optimization function adopted may exhibit many local stationarity points, it strongly depends on the initial assumed conditions and it generally requires high computational time.

A novel calibration-model frame identification technique is proposed in this work, differing from already known approaches (Ewins, 2000; Giuliani et al., 2013; Huynh et al., 2020, 2021; Peumans et al., 2019; Stanbridge and Ewins, 1999; Warren et al., 2011) by only using the standard input/output (I/O) measurements available from the instrument setup. This new technique is also different from these authors previous work (Amadori and Catania, 2021) since it relies on an algebraic approach and on an iterative stabilization procedure.

Since to these authors' knowledge no previous work is known with respect to the identification of the material SLS model order and parameters from estimated $D(\omega)$ in the Δ measured frequency range, a novel identification technique is here proposed. The robustness of these techniques is

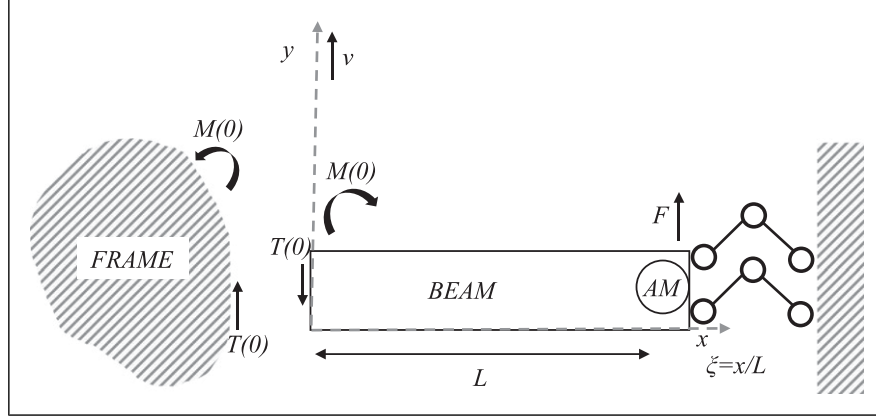


Figure 1. Schematic representation of the instrument frame and beam specimen coupled system model with AM mobile measuring subsystem added m_d mass.

tested by means of some numerically simulated data test cases, taking into account the contribution of added noise, and then some applications of these same techniques in real experimental data test conditions are reported. Results are critically discussed.

2. $D(\omega)$ SLS material model

The material $D(\omega)$ stress($\hat{\sigma}$)–strain($\hat{\varepsilon}$) relationship can be modelled by means of a SLS N order generalized Kelvin model (Amadori and Catania, 2016, 2017; Findley et al., 1989), resulting from series connecting N K-blocks, the i -th block being a parallel connection of an elastic Hooke (E_i parameter) and a viscous Newton (β_i parameter) component, $i = 1, \dots, N$. Since for the i -th block, the following equation holds

$$\hat{\sigma} = (E_i + j \cdot \omega \cdot \beta_i) \cdot \hat{\varepsilon}_i, \quad i = 1, \dots, N \quad (1)$$

it follows that

$$\begin{aligned} \hat{\varepsilon} &= \sum_{i=1}^N \hat{\varepsilon}_i = \hat{\sigma} \cdot \sum_{i=1}^N \frac{1}{E_i + j \cdot \omega \cdot \beta_i} \\ &= \hat{\sigma} \cdot \frac{1}{E_0} \cdot \sum_{i=1}^N \frac{1}{\frac{E_i}{E_0} + j \cdot \omega \cdot \frac{\beta_i}{E_0}} = \hat{\sigma} \cdot \frac{1}{E_0} \cdot \frac{1}{D(\omega)} \end{aligned} \quad (2)$$

where E_0 can be easily experimentally identified from within standard static measurements and $D(\omega)$ estimates can be obtained from dynamical test measurements and the application of an identification technique. The following, highly non-linear, functional dependence of $D(\omega)$ with respect to the SLS material model E_i , β_i , $i = 1, \dots, N$, parameters is outlined in equation (3)

$$D(\omega) = \left(\sum_{i=1}^N \frac{1}{\frac{E_i}{E_0} + j \cdot \omega \cdot \frac{\beta_i}{E_0}} \right)^{-1} \quad (3)$$

so that $(D(\omega))^{-1}$ is expressed in partial fraction form.

From equation (3), the numerical estimate of N , E_i and β_i values from experimental $D(\omega_s)$ estimates, $\omega_s \in \Delta$, appears to be a critical task. A novel algorithm is proposed in this work to obtain a physically sound SLS material model from the $D(\omega)$ rational estimated model, and it will be described in Section 7.

3. Instrument frame-beam coupled experimental system and model assumptions

In this work, a single-cantilever experimental setup (Amadori and Catania, 2016, 2017) is considered. A sinusoidal excitation, whose frequency belongs to a Δ fixed limited range, is applied to a beam specimen of known geometry, and both force and displacement (v) response are measured in correspondence of the same experimental dof. The single experimental degree of freedom (dof) taken into account is the transverse beam displacement at the excited beam end (Amadori and Catania, 2017; Placet and Foltete, 2010), and the beam and mobile measuring system inertial contributions in the Δ range are taken into account.

Figure 1 shows a schematic representation of the instrument-beam specimen coupled mechanical system, and Figure 2 shows the DMA test system used to obtain the measurements presented in Section 9. Free-sliding boundary conditions and a kinematical small displacement and deformation plane field are assumed for a homogeneous-uniform beam specimen. According to the Bernoulli beam theory (Timoshenko et al., 1974)

$$\hat{v}^{iv}(\xi, \omega) - z^4 \cdot \hat{v}(\xi, \omega) = 0; \quad z^4(\omega) = \frac{\rho \cdot S \cdot L^4 \cdot \omega^2}{E_0 \cdot I \cdot D(\omega)} \quad (4)$$

where ρ is the density, S is the section area and I the section moment, L is the beam length and $(\)^i = \partial^i(\) / \partial \xi^i$ is the i -th

derivative with respect to the normalized variable $\zeta = x/L$. It must be outlined that equation (4) takes into full account the inertial contribution of the beam mass distribution. Equation (4) general solution is

$$\begin{aligned} \widehat{v}(\omega, \zeta) &= \bar{\gamma}_1 \cdot \sin(z \cdot \zeta) + \bar{\gamma}_2 \cdot \cos(z \cdot \zeta) + \bar{\gamma}_3 \cdot \sinh(z \cdot \zeta) \\ &+ \bar{\gamma}_4 \cdot \cosh(z \cdot \zeta) \end{aligned} \quad (5)$$

The Fourier transform of θ rotation, T shear and M momentum are (Timoshenko et al., 1974)

$$\begin{aligned} \widehat{\theta}(\omega, \zeta) &= \frac{z}{L} \cdot \widehat{v}'(\omega, \zeta) \\ \widehat{T}(\omega, \zeta) &= \frac{E_0 \cdot I \cdot D(\omega)}{L^3} \cdot \widehat{v}'''(\omega, \zeta) \\ \widehat{M}(\omega, \zeta) &= \frac{E_0 \cdot I \cdot D(\omega)}{L^2} \cdot \widehat{v}''(\omega, \zeta) \end{aligned} \quad (6)$$

Equations (5) and (6) can also be expressed as

$$\begin{aligned} \widehat{v}(\omega, \zeta) &= \lambda_v(\omega, \zeta) \cdot \boldsymbol{\gamma} \cdot F, \\ \lambda_v(\omega, \zeta) &= [\sin(z \cdot \zeta) \quad \cos(z \cdot \zeta) \quad \sinh(z \cdot \zeta) \quad \cosh(z \cdot \zeta)] \\ \widehat{\theta}(\omega, \zeta) &= \lambda_\theta(\omega, \zeta) \cdot \boldsymbol{\gamma} \cdot F, \\ \lambda_\theta(\omega, \zeta) &= \frac{z}{L} \cdot [\cos(z \cdot \zeta) \quad -\sin(z \cdot \zeta) \quad \cosh(z \cdot \zeta) \quad \sinh(z \cdot \zeta)] \\ \widehat{T}(\omega, \zeta) &= \lambda_T(\omega, \zeta) \cdot \boldsymbol{\gamma} \cdot F, \\ \widehat{M}(\omega, \zeta) &= \lambda_M(\omega, \zeta) \cdot \boldsymbol{\gamma} \cdot F, \\ \lambda_T(\omega, \zeta) &= E_0 \cdot I \cdot D(\omega) \cdot \left(\frac{\rho \cdot S \cdot \omega^2}{E_0 \cdot I \cdot D(\omega)} \right)^{\frac{3}{4}} \\ &\cdot [-\cos(z \cdot \zeta) \quad \sin(z \cdot \zeta) \quad \cosh(z \cdot \zeta) \quad \sinh(z \cdot \zeta)] \\ \lambda_M(\omega, \zeta) &= \omega \cdot \sqrt{\rho \cdot S \cdot E_0 \cdot I \cdot D(\omega)} \\ &\cdot [-\sin(z \cdot \zeta) \quad -\cos(z \cdot \zeta) \quad \sinh(z \cdot \zeta) \quad \cosh(z \cdot \zeta)] \\ \boldsymbol{\gamma} &= [\gamma_1 \quad \gamma_2 \quad \gamma_3 \quad \gamma_4]^T; \quad \gamma_i = \frac{\bar{\gamma}_i}{F}, \quad i = 1, \dots, 4 \end{aligned} \quad (7)$$

where $()^T$ is the transpose operator and F is the Fourier transform of the force applied at $\zeta = 1$ and $\boldsymbol{\gamma}$ vector can be found by imposing the boundary conditions with respect to the excitation coupling at $\zeta = 1$ and to the system frame coupling at $\zeta = 0$.

The instrument frame is modelled by means of a two degrees of freedom (2-dofs) model associated to a classical linear second order time domain model, resulting in a 2×2 symmetric matrix $\mathbf{X}(\omega)$ transfer function in the frequency domain

$$\mathbf{X}(\omega) = \begin{bmatrix} X_{(1,1)}(\omega) & X_{(1,2)}(\omega) \\ X_{(1,2)}(\omega) & X_{(2,2)}(\omega) \end{bmatrix} \quad (8)$$

where $\mathbf{X}(\omega)$ components can be modelled by means of the ratio of polynomial functions. $\boldsymbol{\gamma}$ vector then results from the following steps

$$\begin{aligned} \widehat{\theta}(\omega, 1) &= \lambda_\theta(\omega, 1) \cdot \boldsymbol{\gamma} \cdot F = 0 \\ \widehat{T}(\omega, 1) &= \lambda_T(\omega, 1) \cdot \boldsymbol{\gamma} \cdot F = -(F + m_d \cdot \omega^2 \cdot \widehat{v}(1)) \\ \widehat{v}(\omega, 0) &= \lambda_v(\omega, 0) \cdot \boldsymbol{\gamma} \cdot F \\ &= -X_{(1,1)}(\omega) \cdot \widehat{T}(\omega, 0) + X_{(1,2)}(\omega) \cdot \widehat{M}(\omega, 0) \\ \widehat{\theta}(\omega, 0) &= \lambda_\theta(\omega, 0) \cdot \boldsymbol{\gamma} \cdot F \\ &= -X_{(1,2)}(\omega) \cdot \widehat{T}(\omega, 0) + X_{(2,2)}(\omega) \cdot \widehat{M}(\omega, 0) \end{aligned} \quad (9)$$

where m_d is a lumped mass (at $\zeta = 1$) modelling the mobile measuring subsystem inertial contribution. Combining equations (7) and (9), the following equation can be obtained

$$\begin{aligned} \mathbf{AA}(\omega, \mathbf{Xv}(\omega)) \cdot \boldsymbol{\gamma} &= \mathbf{b} \\ \mathbf{AA}(\omega, \mathbf{Xv}(\omega)) &= \begin{bmatrix} \lambda_\theta(\omega, 1) \\ \lambda_T(\omega, 1) + m_d \cdot \omega^2 \cdot \lambda_v(\omega, 1) \\ \lambda_v(\omega, 0) + X_{(1,1)} \cdot \lambda_T(\omega, 0) - X_{(1,2)} \cdot \lambda_M(\omega, 0) \\ \lambda_\theta(\omega, 0) + X_{(1,2)} \cdot \lambda_T(\omega, 0) - X_{(2,2)} \cdot \lambda_M(\omega, 0) \end{bmatrix}, \\ \mathbf{b} &= \begin{Bmatrix} 0 \\ -1 \\ 0 \\ 0 \end{Bmatrix}, \quad \mathbf{Xv}(\omega) = \begin{Bmatrix} X_{(1,1)}(\omega) \\ X_{(1,2)}(\omega) \\ X_{(2,2)}(\omega) \end{Bmatrix} \end{aligned} \quad (10)$$

where vector $\mathbf{Xv}(\omega)$ is defined by means of the different elements of matrix $\mathbf{X}(\omega)$ (equation (8)). From equation (10)

$$\boldsymbol{\gamma} = \mathbf{AA}^{-1}(\omega, \mathbf{Xv}(\omega)) \cdot \mathbf{b} \quad (11)$$

and combining equations (7) and (11), the $h(\omega)$ measurement FRF results as an explicit function of ω and of the instrument frame $\mathbf{X}(\omega)$ model contribution

$$h(\omega) = \frac{\widehat{v}(\omega, 1)}{F} = \lambda_v(\omega, 1) \cdot \mathbf{AA}^{-1}(\omega, \mathbf{Xv}(\omega)) \cdot \mathbf{b} \quad (12)$$

4. System calibration and $\mathbf{X}(\omega)$ identification procedure

A calibration procedure is commonly employed in most test measuring applications to take into account the elastic contribution of the system fixture clamping the fixed end of the beam specimen under test (Figure 2b), generally resulting in only estimating the average system static stiffness with respect to the beam transverse displacement $v(x=0)$ (Figure 1). Such procedure requires the measurement of some reference beam specimens made of known materials.

Nevertheless, such optimal static stiffness value is expected to highly vary with respect to the experimental Δ frequency range, especially if the contribution of instrument frame poles cannot be neglected in such experimental conditions. Moreover, the rotary dynamic frame compliance

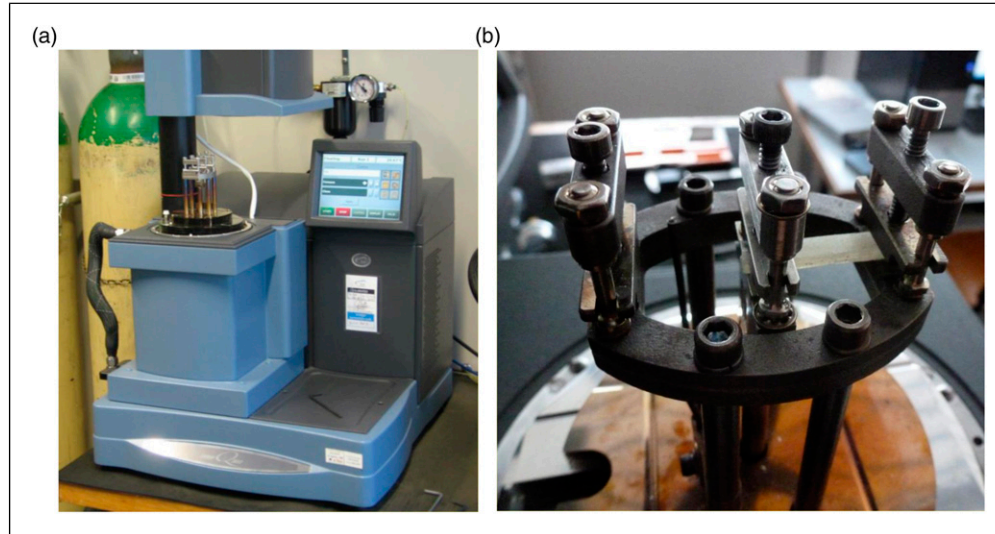


Figure 2. DMA Q800 (TA Instruments) experimental system: (a) instrument; (b) clamping system.

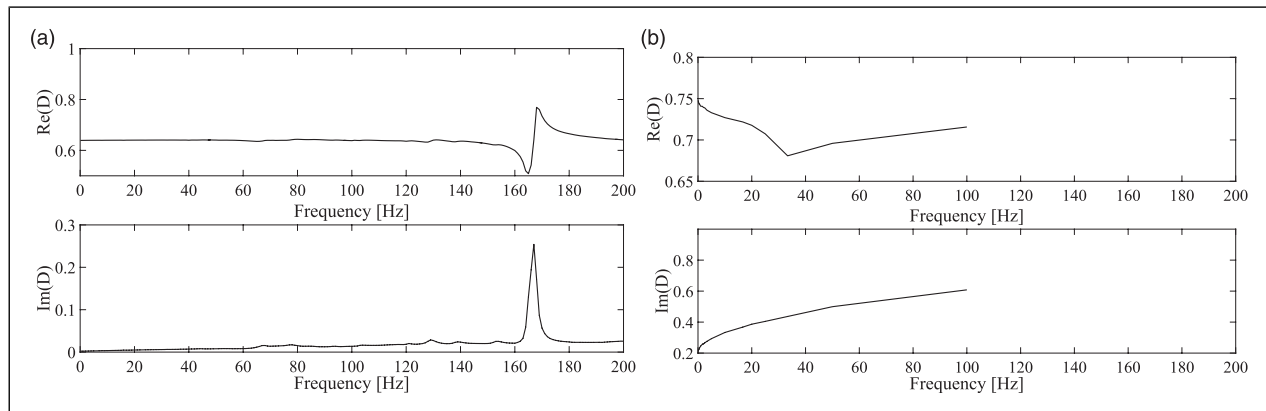


Figure 3. $D(\omega)$ C67 harmonic steel estimate: (a) A setup; (b) B setup.

Table 1. C67 harmonic steel experimental setups.

Setup	DMA instrument	Beam L [mm]	Beam width w [mm]	Beam thickness t [mm]
A	TA Q800	17.5 ± 0.01	12.8 ± 0.01	0.75 ± 0.01
B	NETZSCH 242E Artemis	16.0 ± 0.01	2.97 ± 0.01	0.5 ± 0.01

with respect to beam neutral axis rotation in correspondence of the same beam end position is expected to be also relevant and should be estimated as well.

As a matter of example, Figure 3 shows some experimental results, concerning the $D(\omega)$ identification results related to C67 harmonic steel material (density $\rho = 7850 \text{ kg/m}^3$, $E_0 = 2.1 \cdot 10^{11} \text{ Pa}$), obtained from two different DMA test systems and beam geometries (Table 1) in the same single-cantilever experimental setup. In both setup conditions, frame contribution was taken into account by identifying the frame coupling static transverse stiffness. Experimental conditions are similar for both A and B setups, that is, constant vibration response amplitude (10 μm) at the mobile end of the beam and frequency range

[0.1,200] Hz for one instrument (A setup, Table 1 and Figure 3a), and frequency range [0.1,100] Hz for the other (B setup, Table 1 and Figure 3b). The results are unsatisfactory if compared with the expected (Hooke) model behaviour ($D(\omega)=1$, $E_0 = 2.1 \times 10^{11} \text{ Pa}$), since a low frequency range, low displacement strain and ambient temperature experimental conditions are considered.

In the novel procedure proposed in this work, $\mathbf{X}(\omega)$ can be identified directly from some sets of FRF $h(\omega)$ measurements made on reference specimens. From equation (12), $h(\omega_s)$ measurements, $s = 1, \dots, n_f$, can be compared to their analytical counterparts obtained from within a known beam specimen model coupled to a 2-dofs frame model whose parameters are unknowns. A system of n_f equations

in the frame parameters unknowns is obtained for each tested reference specimen.

Three $X_{11}(\omega)$, $X_{12}(\omega)$ and $X_{22}(\omega)$ unknowns are to be identified at each ω_s frequency value. Assuming a set of $m \geq 3$ different beam specimens, made of known material and geometry, are available for measurement, a set of $(\hat{v}(\omega_s, 1)/F)_i$ measurements, $i = 1, \dots, m$, $s = 1, \dots, n_f$, results. A nonlinear equation system in $\mathbf{Xv}(\omega)$ unknown is obtained

$$\begin{aligned} \left\{ \begin{array}{l} \left(\frac{\hat{v}(\omega_s, 1)}{F} \right)_1 \\ \dots \\ \left(\frac{\hat{v}(\omega_s, 1)}{F} \right)_m \end{array} \right\} &= \left\{ \begin{array}{l} h_1(\omega_s) \\ \dots \\ h_m(\omega_s) \end{array} \right\} \\ &= \left\{ \begin{array}{l} (\lambda_v(\omega_s, 1) \cdot \mathbf{AA}^{-1}(\omega_s, \mathbf{Xv}(\omega_s)))_1 \\ \dots \\ (\lambda_v(\omega_s, 1) \cdot \mathbf{AA}^{-1}(\omega_s, \mathbf{Xv}(\omega_s)))_m \end{array} \right\} \cdot \mathbf{b} \end{aligned} \quad (13)$$

From equation (13), an error vector is defined

$$\begin{aligned} \mathbf{e}(\omega_s, \mathbf{Xv}(\omega_s)) &= \begin{Bmatrix} e_1 \\ \dots \\ e_i \\ \dots \\ e_m \end{Bmatrix} \\ &= \begin{Bmatrix} h_1 - (\lambda_v(\omega_s, 1) \cdot \mathbf{AA}^{-1}(\omega_s, \mathbf{Xv}(\omega_s)))_1 \cdot \mathbf{b} \\ \dots \\ h_i - (\lambda_v(\omega_s, 1) \cdot \mathbf{AA}^{-1}(\omega_s, \mathbf{Xv}(\omega_s)))_i \cdot \mathbf{b} \\ \dots \\ h_m - (\lambda_v(\omega_s, 1) \cdot \mathbf{AA}^{-1}(\omega_s, \mathbf{Xv}(\omega_s)))_m \cdot \mathbf{b} \end{Bmatrix} \\ &\cong \mathbf{0} \end{aligned} \quad (14)$$

In order to find $\mathbf{Xv}(\omega)$ minimizing \mathbf{e} , a two-step approach is adopted. Since equation (14) is highly nonlinear with respect to $\mathbf{Xv}(\omega)$, an approximate model can be obtained by assuming the following approximate boundary conditions, consisting of neglecting the contribution of the distributed beam inertial actions with respect to F and to the inertial contribution of m_d lumped mass

$$\begin{aligned} \hat{v}(\omega, 0) &= \lambda_v(\omega, 0) \cdot \gamma \cdot F = X_{(1,1)}(\omega) \cdot (F + m_d \cdot \omega^2 \cdot \hat{v}(1)) \\ &\quad + X_{(1,2)}(\omega) \cdot (L \cdot F + L \cdot m_d \cdot \omega^2 \cdot \hat{v}(1) + \hat{M}(\omega, 1)) \\ \hat{\theta}(\omega, 0) &= \lambda_\theta(\omega, 0) \cdot \gamma \cdot F = X_{(1,2)}(\omega) \cdot (F + m_d \cdot \omega^2 \cdot \hat{v}(1)) \\ &\quad + X_{(2,2)}(\omega) \cdot (L \cdot F + L \cdot m_d \cdot \omega^2 \cdot \hat{v}(1) + \hat{M}(\omega, 1)) \end{aligned} \quad (15)$$

From equations (7), (9) and (15), the following result is obtained

$$\begin{aligned} \hat{\theta}(\omega_s, 1) &= \bar{\gamma}_1 \cdot \cos(z \cdot \zeta) - \bar{\gamma}_2 \cdot \sin(z \cdot \zeta) + \bar{\gamma}_3 \cdot \cosh(z \cdot \zeta) \\ &\quad + \bar{\gamma}_4 \cdot \sinh(z \cdot \zeta) = 0 \\ \hat{T}(\omega_s, 1) &= \frac{z^3 \cdot E_0 \cdot I \cdot D(\omega_s)}{L^3} \cdot [-\bar{\gamma}_1 \cdot \cos(z \cdot \zeta) + \bar{\gamma}_2 \cdot \sin(z \cdot \zeta) \\ &\quad + \bar{\gamma}_3 \cdot \cosh(z \cdot \zeta) + \bar{\gamma}_4 \cdot \sinh(z \cdot \zeta)] = -F \\ \hat{v}(\omega_s, 0) &= \bar{\gamma}_2 + \bar{\gamma}_4 = X_{(1,1)}(\omega) \cdot F \cdot \mathbf{K}_{In} + X_{(1,2)}(\omega) \cdot L \cdot F \\ &\quad \cdot \mathbf{K}_{In} + X_{(1,2)}(\omega) \cdot \hat{M}(\omega, 1) \\ \hat{\theta}(\omega_s, 0) &= \frac{z}{L} \cdot (\bar{\gamma}_1 + \bar{\gamma}_3) = X_{(1,2)}(\omega) \cdot F \cdot \mathbf{K}_{In} + X_{(2,2)}(\omega) \\ &\quad \cdot L \cdot F \cdot \mathbf{K}_{In} + X_{(2,2)}(\omega) \cdot \hat{M}(\omega, 1) \\ \mathbf{K}_{In} &= \left(1 + m_d \cdot \omega_s^2 \cdot \frac{\hat{v}(\omega_s, 1)}{F} \right) \end{aligned} \quad (16)$$

Equation (16) can be arranged as follows

$$\mathbf{M}(\omega_s, \zeta = 1, \mathbf{Xv}(\omega_s)) \cdot \gamma^0 = \mathbf{N}(\omega_s) \cdot \mathbf{Xv}(\omega_s) - \mathbf{b}_a(\omega_s)$$

$$\gamma^0 = [\gamma_1^0 \quad \gamma_2^0 \quad \gamma_3^0 \quad \gamma_4^0]^T; \quad \gamma_r^0 = \frac{\bar{\gamma}_r}{F \cdot \mathbf{K}_{In}}, \quad r = 1, \dots, 4$$

$$\mathbf{M}(\omega_s, 1, \mathbf{Xv}(\omega_s)) = \begin{bmatrix} \cos(z) & -\sin(z) & \cosh(z) & \sinh(z) \\ -D(\omega) \cdot z^3 \cdot \cos(z) & D(\omega) \cdot z^3 \cdot \sin(z) & D(\omega) \cdot z^3 \cdot \cosh(z) & D(\omega) \cdot z^3 \cdot \sinh(z) \\ \sin(z) \cdot P \cdot X_{(1,2)} & 1 + \cos(z) \cdot P \cdot X_{(1,2)} & -\sinh(z) \cdot P \cdot X_{(1,2)} & 1 - \cosh(z) \cdot P \cdot X_{(1,2)} \\ \frac{z}{L} + \sin(z) \cdot P \cdot X_{(2,2)} & \cos(z) \cdot P \cdot X_{(2,2)} & \frac{z}{L} - \sinh(z) \cdot P \cdot X_{(2,2)} & -\cosh(z) \cdot P \cdot X_{(2,2)} \end{bmatrix}$$

$$\mathbf{N}(\omega_s) = \begin{bmatrix} 0 & 0 & 0 \\ 0 & 0 & 0 \\ 1 & L & 0 \\ 0 & 1 & L \end{bmatrix}, \quad \mathbf{b}_a(\omega_s) = \begin{bmatrix} 0 \\ -\frac{L^3}{E_0 \cdot I} \\ 0 \\ 0 \end{bmatrix}, \quad P = \frac{z^2 \cdot E_0 \cdot I \cdot D(\omega_s)}{L^2}$$

(17)

From measurement on the i -th specimen

$$\gamma^0 = \left(\mathbf{M}^{-1}(\omega_s, 1, \mathbf{Xv}(\omega_s)) \cdot \mathbf{N}(\omega_s) \cdot \mathbf{Xv}(\omega_s) + \mathbf{M}^{-1}(\omega_s, 1, \mathbf{Xv}(\omega_s)) \cdot \mathbf{b}_a(\omega_s) \right)_i \quad (18)$$

The i -th specimen FRF measurement estimate, $i = 1, \dots, m$, can be expressed as

$$h_i(\omega_s) = \left(K_{In} \cdot \lambda_v(\omega_s, 1) \cdot \left(\mathbf{M}^{-1}(\omega_s, 1, \mathbf{Xv}(\omega_s)) \cdot \mathbf{N}(\omega_s) \cdot \mathbf{Xv}(\omega_s) + \mathbf{M}^{-1}(\omega_s, 1, \mathbf{Xv}(\omega_s)) \cdot \mathbf{b}_a(\omega_s) \right) \right)_i \quad (19)$$

Manipulating equation (19)

$$\begin{aligned} (AA_a)_i(\omega_s, \mathbf{Xv}(\omega_s)) \cdot \mathbf{Xv}(\omega_s) &= (bb_a)_i(\omega_s, \mathbf{Xv}(\omega_s)) \\ (bb_a)_i(\omega_s, \mathbf{Xv}(\omega_s)) &= \left(\frac{h(\omega_s)}{K_{In}} - \lambda_v(\omega_s, 1) \cdot \mathbf{M}^{-1}(\omega_s, 1, \mathbf{Xv}(\omega_s)) \cdot \mathbf{b}_a(\omega_s) \right)_i \\ (AA_a)_i(\omega_s, \mathbf{Xv}(\omega_s)) &= \left(\lambda_v(\omega_s, 1) \cdot \mathbf{M}^{-1}(\omega_s, 1, \mathbf{Xv}(\omega_s)) \cdot \mathbf{N}(\omega_s) \cdot \mathbf{Xv}(\omega_s) \right)_i \end{aligned} \quad (20)$$

And in compact matrix form, taking into account all m beam specimen contributions

$$\begin{aligned} \mathbf{AA}_a(\omega_s, \mathbf{Xv}(\omega_s)) \cdot \mathbf{Xv}(\omega_s) &= \mathbf{bb}_a(\omega_s, \mathbf{Xv}(\omega_s)) \\ \mathbf{bb}_a(\omega_s, \mathbf{Xv}(\omega_s)) &= \left\{ \begin{array}{c} \left(\frac{h(\omega_s)}{K_{In}} \right)_1 - \left(\lambda_v(\omega_s, 1) \cdot \mathbf{M}^{-1}(\omega_s, 1, \mathbf{Xv}(\omega_s)) \cdot \mathbf{b}_a(\omega_s) \right)_1 \\ \dots \\ \left(\frac{h(\omega_s)}{K_{In}} \right)_m - \left(\lambda_v(\omega_s, 1) \cdot \mathbf{M}^{-1}(\omega_s, 1, \mathbf{Xv}(\omega_s)) \cdot \mathbf{b}_a(\omega_s) \right)_m \end{array} \right\} \\ \mathbf{AA}_a(\omega_s, \mathbf{Xv}(\omega_s)) &= \left\{ \begin{array}{c} \left(\lambda_v(\omega_s, 1) \cdot \mathbf{M}^{-1}(\omega_s, 1, \mathbf{Xv}(\omega_s)) \cdot \mathbf{N}(\omega_s) \right)_1 \\ \dots \\ \left(\lambda_v(\omega_s, 1) \cdot \mathbf{M}^{-1}(\omega_s, 1, \mathbf{Xv}(\omega_s)) \cdot \mathbf{N}(\omega_s) \right)_m \end{array} \right\} \end{aligned} \quad (21)$$

The following iterative procedure is proposed to evaluate \mathbf{Xv}

$$\begin{aligned} \mathbf{Xv}_0 &= \mathbf{0} \\ \mathbf{Xv}_k &= \mathbf{AA}_a^{-1}(\omega_s, \mathbf{Xv}_{k-1}(\omega_s)) \cdot \mathbf{bb}_a(\omega_s, \mathbf{Xv}_{k-1}(\omega_s)) \end{aligned} \quad (22)$$

where index k is the iteration number. The end condition for the iterative procedure of equation (22) is

$$\begin{aligned} \mathbf{Xv}(\omega_s) &= \mathbf{Xv}_k(\omega_s) \quad : \quad \mathbf{e}^*(\omega_s, \mathbf{Xv}_k(\omega_s)) \cdot \mathbf{e}(\omega_s, \mathbf{Xv}_k(\omega_s)) \\ &< \text{tol}_e \quad \text{OR} \quad |\mathbf{Xv}_k(\omega_s) - \mathbf{Xv}_{k-1}(\omega_s)| < \text{tol}_y. \end{aligned} \quad (23)$$

Since the numerical inversion of \mathbf{AA}_a $m \times 3$ matrix can be critical in some iterative steps, a matrix inversion procedure based on the Svd (Forsythe et al., 1977) decomposition,

lowering the matrix rank from three to two and obtaining the solution associated to \mathbf{Xv} minimal norm, is here adopted with good results. It also appears that the numerical rank associated to \mathbf{AA}_a , formally evaluated by means of the singular values obtained from applying the Svd procedure to \mathbf{AA}_a , depends on the correct choice of the m test reference beam specimens, meaning that additional test specimen measurements could be added to the current reference set to increase the \mathbf{AA}_a rank.

Since in most cases equation (22) contraction requirements hold (Cacioppoli, 1930; Granas and Dugundji, 2003), convergence can be obtained with only a few iterations. When such conditions do not hold, error from equation (14) can be approximated by means of a first order Taylor expansion, and a new iterative procedure, evaluated from within the exact model boundary conditions (equation (9)), starting from the approximate value obtained from the previously defined iterative procedure, can be defined as follows

$$\begin{aligned} \mathbf{Xv}_k(\omega_s) &= \mathbf{Xv}_{k-1}(\omega_s) - \left(\frac{\partial \mathbf{e}}{\partial \mathbf{Xv}}(\omega_s, \mathbf{Xv}_{k-1}(\omega_s)) \right)^{-1} \\ &\cdot \mathbf{e}(\omega_s, \mathbf{Xv}_{k-1}(\omega_s)) \end{aligned} \quad (24)$$

where

$$\frac{\partial \mathbf{e}}{\partial \mathbf{Xv}}(\omega_s, \mathbf{Xv}(\omega_s)) = \begin{bmatrix} \frac{\partial e_1}{\partial X_{(1,1)}} & \frac{\partial e_1}{\partial X_{(1,2)}} & \frac{\partial e_1}{\partial X_{(2,2)}} \\ \dots & \dots & \dots \\ \frac{\partial e_i}{\partial X_{(1,1)}} & \frac{\partial e_i}{\partial X_{(1,2)}} & \frac{\partial e_i}{\partial X_{(2,2)}} \\ \dots & \dots & \dots \\ \frac{\partial e_m}{\partial X_{(1,1)}} & \frac{\partial e_m}{\partial X_{(1,2)}} & \frac{\partial e_m}{\partial X_{(2,2)}} \end{bmatrix},$$

$$\frac{\partial e_i}{\partial X_{(r,l)}} = -\lambda_v(\omega_s, 1) \cdot \left(\frac{\partial \mathbf{AA}^{-1}}{\partial X_{(r,l)}}(\omega_s, \mathbf{Xv}(\omega_s)) \right)_i \cdot \mathbf{b}$$

$$\begin{aligned} \left(\frac{\partial \mathbf{AA}^{-1}}{\partial X_{(r,l)}}(\omega_s, \mathbf{Xv}(\omega_s)) \right)_i &= -(\mathbf{AA}^{-1}(\omega_s, \mathbf{Xv}(\omega_s)))_i \\ &\cdot \left(\frac{\partial \mathbf{AA}}{\partial X_{(r,l)}}(\omega_s, \mathbf{Xv}(\omega_s)) \right)_i \cdot (\mathbf{AA}^{-1}(\omega_s, \mathbf{Xv}(\omega_s)))_i \end{aligned}$$

$$\frac{\partial (\mathbf{AA}(\omega_s, \mathbf{Xv}(\omega_s)))_i}{\partial X_{(1,1)}} = [\mathbf{0} \quad \mathbf{0} \quad \lambda_{\mathbf{T}}(\omega_s, 1) \quad \mathbf{0}]$$

$$\frac{\partial (\mathbf{AA}(\omega_s, \mathbf{Xv}(\omega_s)))_i}{\partial X_{(1,2)}} = [\mathbf{0} \quad \mathbf{0} \quad -\lambda_{\mathbf{M}}(\omega_s, 1) \quad \lambda_{\mathbf{T}}(\omega_s, 1)]$$

$$\frac{\partial (\mathbf{AA}(\omega_s, \mathbf{Xv}(\omega_s)))_i}{\partial X_{(2,2)}} = [\mathbf{0} \quad \mathbf{0} \quad \mathbf{0} \quad -\lambda_{\mathbf{M}}(\omega_s, 1)].$$

(25)

Iterations end when the conditions defined in equation (23) hold.

5. $\mathbf{X}(\omega)$ rational function model identification

The instrument frame frequency transfer function vector $\mathbf{Xv}(\omega_s)$ can be associated to a classical second order model which includes the two previously defined coupling dofs. Such model can be mathematically described in the Δ frequency domain by means of a transfer matrix whose components are defined by the ratio of an o_F order to an o_F+1 order polynomial function (Ewins, 2000)

$$X_{(r,l)}(j \cdot \omega_s) = \frac{a_{o_F-1}^{(r,l)} \cdot p_{o_F-1}(j \cdot \omega_s) + \dots + a_i^{(r,l)} \cdot p_i(j \cdot \omega_s) + \dots + a_0^{(r,l)} \cdot p_0(j \cdot \omega_s)}{q_{o_F}(j \cdot \omega_s) + \dots + d_g \cdot q_g(j \cdot \omega_s) + \dots + d_0 \cdot q_0(j \cdot \omega_s)} \quad (26)$$

$$[p_0(j \cdot \omega) \quad p_1(j \cdot \omega) \quad \dots \quad p_{o_F-1}(j \cdot \omega)] \cdot \mathbf{a}^{(r,l)} +$$

$$- [X_{(r,l)}(j \cdot \omega) \cdot q_0(j \cdot \omega) \quad X_{(r,l)}(j \cdot \omega) \cdot q_1(j \cdot \omega) \quad \dots \quad X_{(r,l)}(j \cdot \omega) \cdot q_{o_F-1}(j \cdot \omega)] \cdot \mathbf{d} = X_{(r,l)} \cdot q_{o_F}(j \cdot \omega),$$

$$\mathbf{a}^{(r,l)} = \begin{Bmatrix} a_0^{(r,l)} \\ \dots \\ a_{o_F-1}^{(r,l)} \end{Bmatrix}; \quad \mathbf{d} = \begin{Bmatrix} d_0 \\ \dots \\ d_{o_F-1} \end{Bmatrix}$$

where $p_i(j\omega)$, $i = 0, \dots, o_F-1$, and $q_g(j\omega)$, $g = 0, \dots, o_F$, are polynomials from a known polynomial base, for example, monomial, Legendre, Chebyshev, Forsythe among all (Allemang and Phillips, 2004; Bogatyrev, 2010; Dankovic et al., 2009; Forsythe 1957; Kelly, 1967;

1957; Kelly, 1967; Phillips et al., 2011; Richardson and Formenti, 1982).

To increase the numerical accuracy, the frequency values are normalized so that $0 < \omega_s < 1$ is assumed. From equation (26)

$$\begin{aligned} & [q_{o_F}(j \cdot \omega_s) + d_{o_F-1} \cdot q_{o_F-1}(j \cdot \omega_s) + \dots + d_g \cdot q_g(j \cdot \omega_s) \\ & + \dots + d_0 \cdot q_0(j \cdot \omega_s)] \cdot X_{(r,l)}(j \cdot \omega_s) = \\ & = a_{o_F-1}^{(r,l)} \cdot p_{o_F-1}(j \cdot \omega_s) + \dots + a_i^{(r,l)} \cdot p_i(j \cdot \omega_s) \\ & + \dots + a_0^{(r,l)} \cdot p_0(j \cdot \omega_s) \end{aligned} \quad (27)$$

and in compact form

where $\mathbf{a}^{(r,l)}$ and \mathbf{d} are both real vectors, that is

$$\mathbf{a}^{(r,l)}, \mathbf{d} \in \mathfrak{R}^{o_F} \quad (29)$$

The following matrices are defined

$$\begin{aligned} \mathbf{p} &= \begin{Bmatrix} p_0(j \cdot \omega_1) & p_1(j \cdot \omega_1) & \dots & p_{o_F-1}(j \cdot \omega_1) \\ \dots & \dots & \dots & \dots \\ p_0(j \cdot \omega_{n_f}) & p_1(j \cdot \omega_{n_f}) & \dots & p_{o_F-1}(j \cdot \omega_{n_f}) \end{Bmatrix}; \quad \mathbf{vv}^{(r,l)} = \begin{Bmatrix} X_{(r,l)}(j \cdot \omega_1) \cdot q_{o_F}(j \cdot \omega_1) \\ \dots \\ X_{(r,l)}(j \cdot \omega_{n_f}) \cdot q_{o_F}(j \cdot \omega_{n_f}) \end{Bmatrix} \\ \mathbf{XX}^{(r,l)} &= \begin{Bmatrix} X_{(r,l)}(j \cdot \omega_1) \cdot q_0(j \cdot \omega_1) & X_{(r,l)}(j \cdot \omega_1) \cdot q_1(j \cdot \omega_1) & \dots & X_{(r,l)}(j \cdot \omega_1) \cdot q_{o_F-1}(j \cdot \omega_1) \\ \dots & \dots & \dots & \dots \\ X_{(r,l)}(j \cdot \omega_{n_f}) \cdot q_0(j \cdot \omega_{n_f}) & X_{(r,l)}(j \cdot \omega_{n_f}) \cdot q_1(j \cdot \omega_{n_f}) & \dots & X_{(r,l)}(j \cdot \omega_{n_f}) \cdot q_{o_F-1}(j \cdot \omega_{n_f}) \end{Bmatrix} \\ \mathbf{aa} &= [\mathbf{a}^{(1,1)} \quad \mathbf{a}^{(1,2)} \quad \mathbf{a}^{(2,2)}]^T \in \mathfrak{R}^{3 \times o_F} \end{aligned} \quad (30)$$

Richardson and Formenti, 1982), and $(r,l) = (1,1), (1,2)$ or $(2,2)$ refers to the indexes of $\mathbf{X}(\omega_s)$ matrix and $\mathbf{Xv}(\omega_s)$ vector elements.

The parameters $a_i^{(r,l)}$ and d_g (equation (26)) associated to the $\mathbf{X}(\omega)$ rational model can be identified by means of a standard approach (Allemang and Phillips, 2004; Forsythe

$$\begin{cases} [\mathbf{p} & \mathbf{0} & \mathbf{0}] \cdot \mathbf{aa} - \mathbf{XX}^{(1,1)} \cdot \mathbf{d} = \mathbf{vv}^{(1,1)} \\ [\mathbf{0} & \mathbf{p} & \mathbf{0}] \cdot \mathbf{aa} - \mathbf{XX}^{(1,2)} \cdot \mathbf{d} = \mathbf{vv}^{(1,2)} \\ [\mathbf{0} & \mathbf{0} & \mathbf{p}] \cdot \mathbf{aa} - \mathbf{XX}^{(2,2)} \cdot \mathbf{d} = \mathbf{vv}^{(2,2)} \end{cases} \quad (31)$$

In compact form

$$\Lambda \cdot \mathbf{aa} - \Theta \cdot \mathbf{d} = \Omega,$$

$$\Lambda = \text{diag}(\mathbf{p}); \quad \Theta = \begin{bmatrix} \mathbf{XX}^{(1,1)} \\ \mathbf{XX}^{(1,2)} \\ \mathbf{XX}^{(2,2)} \end{bmatrix}; \quad \Omega = \begin{bmatrix} \mathbf{vv}^{(1,1)} \\ \mathbf{vv}^{(1,2)} \\ \mathbf{vv}^{(2,2)} \end{bmatrix} \quad (32)$$

From equation (32) \mathbf{ee} error vector and Φ optimal functional can be defined

$$\begin{aligned} \mathbf{ee} &= \Lambda \cdot \mathbf{aa} - \Theta \cdot \mathbf{d} - \Omega \\ \Phi &= \frac{1}{2} \cdot \mathbf{ee}^* \cdot \mathbf{ee} \end{aligned} \quad (33)$$

By applying the stationarity condition, and taking into account the equation (29) condition

$$\begin{cases} \frac{\partial \Phi}{\partial \mathbf{aa}} = \text{Re}(\Lambda^* \cdot \Lambda) \cdot \mathbf{aa} - \text{Re}(\Lambda^* \cdot \Theta) \cdot \mathbf{d} - \text{Re}(\Lambda^* \cdot \Omega) = \mathbf{0} \\ \frac{\partial \Phi}{\partial \mathbf{d}} = \text{Re}(\Theta^* \cdot \Theta) \cdot \mathbf{d} - \text{Re}(\Lambda^* \cdot \Theta)^T \cdot \mathbf{aa} + \text{Re}(\Theta^* \cdot \Omega) = \mathbf{0} \end{cases} \quad (34)$$

where $\text{Re}(\cdot)$ and $\text{Im}(\cdot)$ are the real part and imaginary part operators. From equation (34), unknown model \mathbf{aa} and \mathbf{d} model parameters result

$$\begin{cases} \mathbf{aa} = (\text{Re}(\Lambda^* \cdot \Lambda))^{-1} \cdot (\text{Re}(\Lambda^* \cdot \Theta) \cdot \mathbf{d} + \text{Re}(\Lambda^* \cdot \Omega)) \\ \mathbf{d} = (\text{Re}(\Theta^* \cdot \Theta) - \text{Re}(\Lambda^* \cdot \Theta)^T \cdot (\text{Re}(\Lambda^* \cdot \Lambda))^{-1} \cdot \text{Re}(\Lambda^* \cdot \Theta))^{-1} \\ \quad \cdot (\text{Re}(\Lambda^* \cdot \Theta)^T \cdot (\text{Re}(\Lambda^* \cdot \Lambda))^{-1} \\ \quad \cdot (\text{Re}(\Lambda^* \cdot \Omega)) - \text{Re}(\Theta^* \cdot \Omega)) \end{cases} \quad (35)$$

Equation (26) can also be expressed in partial fraction form as in equation (36)

$$\begin{aligned} X_{(r,l)}(j \cdot \omega_s) &= \frac{a_{o_F-1}^{(r,l)} \cdot p_{o_F-1}(j \cdot \omega_s) + \dots + a_1^{(r,l)} \cdot p_1(j \cdot \omega_s) + a_0^{(r,l)} \cdot p_0(j \cdot \omega_s)}{\prod_{k=1}^{o_F} (j\omega_s - \mu_k)} \\ &= \sum_{k=1}^{o_F} \frac{R_k}{(j\omega_s - \mu_k)} \end{aligned} \quad (36)$$

where index k refers to poles and residues ($k = 1, \dots, o_F$), the μ_k poles are the zeros of the $X_{(r,l)}(\omega)$ denominator and the R_k residues can be evaluated from equation (36)

$$R_k = \frac{a_{o_F-1}^{(r,l)} \cdot p_{o_F-1}(\mu_k) + \dots + a_1^{(r,l)} \cdot p_1(\mu_k) + a_0^{(r,l)} \cdot p_0(\mu_k)}{\prod_{i=1, i \neq k}^{o_F} (\mu_k - \mu_i)} \quad (37)$$

R_k residues and μ_k poles are expected to appear as complex conjugated pairs or real values. Accurate and physically sound $\mathbf{X}(\omega)$ model can be obtained by discarding unphysical poles and their associated residues, for example, poles with positive real part or couples of complex conjugate poles associated to natural frequency (the norm of such poles) external to the frequency excitation range, so that the optimal o_F model order value naturally results by applying this procedure. Numerically unstable poles, that is, poles meaningfully varying when further evaluated by increasing the assumed o_F model order, can be discarded (Amadori and Catania, 2017; Ewins, 2000), with their associated residues, as well. The mean contribution of the discarded pole-residue couples is taken into account by means of the evaluation of a third-grade polynomial function and also adding it to the main rational identified function (Ewins, 2000).

The effect of the choice of the $p_r(j \cdot \omega)$, $q_g(j \cdot \omega)$, polynomial bases was also investigated and rational fits made with the Legendre polynomial basis generally produced the most effective results. The Legendre polynomial basis is thus used herein in all of the applications presented in this work.

6. Material $\mathbf{D}(\omega)$ estimate

Starting from $h(\omega_s)$, $s = 1, \dots, n_{fs}$ measurement estimates obtained from a beam specimen of unknown material model, $\mathbf{X}(\omega)$ being known from the application of the procedure outlined in Section 5, from equation (12) the following nonlinear vector equation with respect to $\mathbf{Dv}(\omega)$ unknown vector holds

An iterative approach, based on the Taylor series approximation of $\mathbf{ev}_{\mathbf{D}}(\omega_s)$ error, defined in equation (38), assuming $\omega_1 \rightarrow 0$, is adopted

$$\begin{aligned} \mathbf{Dv}_k(\omega_s) &= \mathbf{Dv}_{k-1}(\omega_s) - \left(\frac{\partial \mathbf{ev}_{\mathbf{D}}}{\partial \mathbf{Dv}}(\omega_s, \mathbf{Dv}_{k-1}(\omega_s)) \right)^{-1} \\ &\quad \cdot \mathbf{ev}_{\mathbf{D}}(\omega_s, \mathbf{Dv}_{k-1}(\omega_s)), \\ \mathbf{Dv}_0(\omega_s) &= \mathbf{Dv}(\omega_{s-1}), \\ \mathbf{Dv}_0(\omega_1) &= [1 \quad 0]^T \end{aligned} \quad (39)$$

with end condition

$$\begin{aligned} \mathbf{Dv}(\omega_s) = \mathbf{Dv}_k(\omega_s) : \mathbf{ev}_{\mathbf{D}}^*(\omega_s, \mathbf{Dv}_k(\omega_s)) \\ \cdot \mathbf{ev}_{\mathbf{D}}(\omega_s, \mathbf{Dv}_k(\omega_s)) < \text{tol}_e \\ \text{OR } |\mathbf{Dv}_k(\omega_s) - \mathbf{Dv}_{k-1}(\omega_s)| < \text{tol}_D \end{aligned} \quad (40)$$

From Cauchy–Riemann condition equations (Shilov, 1996)

$$\begin{aligned} \mathbf{Dv}(\omega_s) &= [\text{Re}(D(\omega_s)) \quad \text{Im}(D(\omega_s))]^T \\ \mathbf{ev}_{\mathbf{D}}(\omega_s) &= \begin{cases} \text{Re}(\lambda_{\mathbf{v}}(\omega_s, 1, \mathbf{Dv}(\omega_s)) \cdot \mathbf{AA}^{-1}(\omega, \mathbf{Dv}(\omega_s)) \cdot \mathbf{b}) - \text{Re}(h(\omega_s)) \\ \text{Im}(\lambda_{\mathbf{v}}(\omega_s, 1, \mathbf{Dv}(\omega_s)) \cdot \mathbf{AA}^{-1}(\omega, \mathbf{Dv}(\omega_s)) \cdot \mathbf{b}) - \text{Im}(h(\omega_s)) \end{cases} \end{aligned} \quad (38)$$

$$\frac{\partial \mathbf{e}_{\mathbf{D}}}{\partial \mathbf{D}\mathbf{v}} = \begin{bmatrix} \operatorname{Re}\left(\frac{\partial e_D}{\partial D}\right) & -\operatorname{Im}\left(\frac{\partial e_D}{\partial D}\right) \\ \operatorname{Im}\left(\frac{\partial e_D}{\partial D}\right) & \operatorname{Re}\left(\frac{\partial e_D}{\partial D}\right) \end{bmatrix} \quad (41)$$

where

$$\begin{aligned} \frac{\partial e_D}{\partial D} &= \frac{\partial \lambda_v(\omega_s, 1)}{\partial z} \cdot \frac{\partial z}{\partial D} \cdot \mathbf{A}\mathbf{A}^{-1} \cdot \mathbf{b} + \lambda_v(\omega_s, 1) \cdot \frac{\partial \mathbf{A}\mathbf{A}^{-1}}{\partial D} \cdot \mathbf{b} \\ \frac{\partial \lambda_v(\omega_s, 1)}{\partial z} &= [\cos(z) \quad -\sin(z) \quad \cosh(z) \quad \sinh(z)] \\ \frac{\partial z}{\partial D} &= -\frac{1}{4} \cdot \left(\frac{\rho \cdot S \cdot L^2 \cdot \omega_s^2}{E_0 \cdot I} \right)^{\frac{1}{4}} \cdot D(\omega_s)^{-\frac{5}{4}} \\ \frac{\partial \mathbf{A}\mathbf{A}^{-1}}{\partial D} &= -\mathbf{A}\mathbf{A}^{-1} \cdot \frac{\partial \mathbf{A}\mathbf{A}}{\partial D} \cdot \mathbf{A}\mathbf{A}^{-1} \\ \frac{\partial \mathbf{A}\mathbf{A}}{\partial D} &= \begin{bmatrix} \frac{\partial \lambda_\theta(\omega_s, 1)}{\partial z} \cdot \frac{\partial z}{\partial D} \\ \frac{\partial \lambda_T(\omega_s, 1)}{\partial D} + m_d \cdot \omega_s^2 \cdot \frac{\partial \lambda_v(\omega_s, 1)}{\partial z} \cdot \frac{\partial z}{\partial D} \\ X_{(1,1)}(\omega_s) \cdot \frac{\partial \lambda_T(\omega_s, 1)}{\partial D} - X_{(1,2)}(\omega_s) \cdot \frac{\partial \lambda_M(\omega_s, 1)}{\partial D} \\ \frac{\partial \lambda_\theta(\omega_s, 1)}{\partial D} + X_{(1,2)}(\omega_s) \cdot \frac{\partial \lambda_T(\omega_s, 1)}{\partial D} - X_{(2,2)}(\omega_s) \cdot \frac{\partial \lambda_M(\omega_s, 1)}{\partial D} \end{bmatrix} \end{aligned} \quad (42)$$

Since from equation (3), the reciprocal of $D(\omega)$ can be modelled by means of a partial fraction sum; an equivalent polynomial rational function form can be assumed as well

$$\begin{aligned} \frac{1}{D(\omega)} &= \frac{a_{o-1} \cdot (j \cdot \omega)^{o-1} + \dots + a_1 \cdot (j \cdot \omega) + a_0}{(j \cdot \omega)^o + \dots + d_1 \cdot (j \cdot \omega) + d_0} \\ &= \frac{\prod_{k=0}^{o-1} a_k \cdot (j \cdot \omega)^k}{\prod_{i=0}^o d_i \cdot (j \cdot \omega)^i}; \quad (a_0 = d_0 \equiv 1; \quad o \equiv N) \end{aligned} \quad (43)$$

Equation (43) refers to the ratio of polynomials, formally equivalent to equation (26) where $a_0 = d_0 = 1$ result since $D(0) = 1$ and monomial basis $p_k(j \cdot \omega) = (j \cdot \omega)^k$ and $q_i(j \cdot \omega) = (j \cdot \omega)^i$ are outlined but the Legendre polynomial basis was mainly adopted for the sake of effectiveness. The identification procedure previously defined in Section 4, being o the unknown polynomial order, can be used in this context to identify the a_k and d_i coefficients.

7. $D(\omega)$ standard linear solid model identification

The material SLS model parameters can be easily evaluated from the a_k and d_i parameters obtained from the previously outlined procedure. From equation (3) equation (44) also results

$$\begin{aligned} \frac{1}{D(\omega)} &= \sum_{i=1}^N \frac{\frac{E_0}{\beta_i}}{j \cdot \omega - \left(-\frac{E_i}{\beta_i} \right)} \\ &= \sum_{i=1}^N \frac{R_i}{j \cdot \omega - \mu_i} = \frac{\prod_{k=0}^{o-1} a_k \cdot (j \cdot \omega)^k}{\prod_{i=0}^o d_i \cdot (j \cdot \omega)^i} \end{aligned} \quad (44)$$

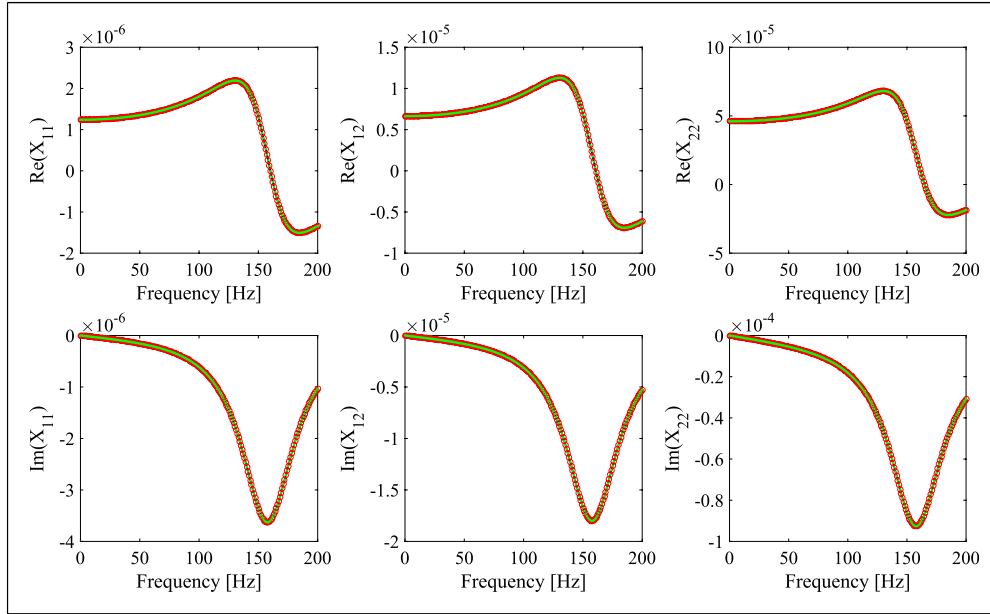
μ_i poles are the zeros of the polynomial equation associated to d_i coefficients, and R_i residues are evaluated using equation (37). Since the $1/D(\omega)$ identified model must be physically sound, the optimal N model order number, coincident with the identified SLS model order, is evaluated by iteratively assuming increasing o values and evaluating pole stability diagrams as illustrated in Section 5 and taking into account only the stable, negative real poles and associated positive real residues.

From equation (44)

$$\begin{cases} N = o \quad \text{stable} \\ E_i = -\mu_i \cdot \frac{E_0}{R_i} \\ \beta_i = \frac{E_0}{R_i} \end{cases} \quad (45)$$

Table 2. Numerical test case beam models.

Specimen	L [mm]	Width w [mm]	Thickness t [mm]	ρ [kg/m ³]	N	E_i [Pa]	β_i [Pa·s]
T	280	100	15	7850	1	$2.1 \cdot 10^{11}$	$7 \cdot 10^7$
C1	28	12.7	3	7850	1	$2.1 \cdot 10^{11}$	0
C2	32	12.7	3	7850	1	$2.1 \cdot 10^{11}$	0
C3	38	12.7	3	7850	1	$2.1 \cdot 10^{11}$	0
D1	17.5	6	0.75	7850	2	$3.8 \cdot 10^{10}$ $4.3 \cdot 10^{10}$	$1.9 \cdot 10^8$ $1.1 \cdot 10^7$

**Figure 4.** $\bar{X}(\omega)$ reference model (black); $\mathbf{X}(\omega)$ estimated values from virtual measurements with no added noise (red) and rational fit (green).

8. Numerically simulated test measurements

Some numerical test cases are presented in order to test the accuracy of the identification procedure. A reference $\bar{X}(\omega)$ model is analytically found by modelling the instrument frame as a homogeneous uniform beam with normal clamped-sliding boundary conditions (beam T, Table 2), whose material is modelled by a Kelvin material model ($N = 1$ SLS model), (Figures 4 and 5, black line). $\mathbf{X}(\omega)$ is then numerically identified from within the numerically simulated response data, taking into account noise, generated from three uniform homogeneous beam (beam C1, C2 and C3, Table 2) with a Hooke material model ($D(\omega) = 1$) coupled to $\bar{X}(\omega)$. Measurement noise is taken into account by adding random noise to the $h(\omega)$ FRF measurements obtained from reference beams C1–C3 coupled with the frame analytical model.

The estimated $\mathbf{X}(\omega)$ elements resulting from simulated measurements without noise are shown in Figure 4, and it

appears that $\mathbf{X}(\omega)$ estimates coincide with reference $\bar{X}(\omega)$ model. Figure 5 shows the $\mathbf{X}(\omega)$ identification results from simulated measurements with noise, $S/N = 80$ dB ($S/N \geq 80$ dB can be typically expected in accurate experimental test results). It results from Figure 5 that while identified $X_{(1,1)}(\omega)$ is practically coincident with reference $\bar{X}_{(1,1)}(\omega)$, the error associated to identified $X_{(1,2)}(\omega)$ and $X_{(2,2)}(\omega)$ with respect to references appears to be high. Nevertheless, by comparing the $h(\omega)$ simulated measurements obtained from within C1–C3 data specimen and the identified $\mathbf{X}(\omega)$ model with the same data used to identify $\mathbf{X}(\omega)$, shown in Figure 6, it appears that the global effect of such errors on $h(\omega)$ is minimal. Geometric and material data (model $\bar{D}(\omega)$) related to D1 beam, reported in Table 2, are used to numerically simulate the response of the beam coupled to $\bar{X}(\omega)$, taking into account of the contribution of numerically generated noise ($S/N = 80$ dB). $D(\omega)$ is identified and the results are presented in Figure 7 and Table 3. It appears that identification results are practically coincident with reference values when simulated noise is

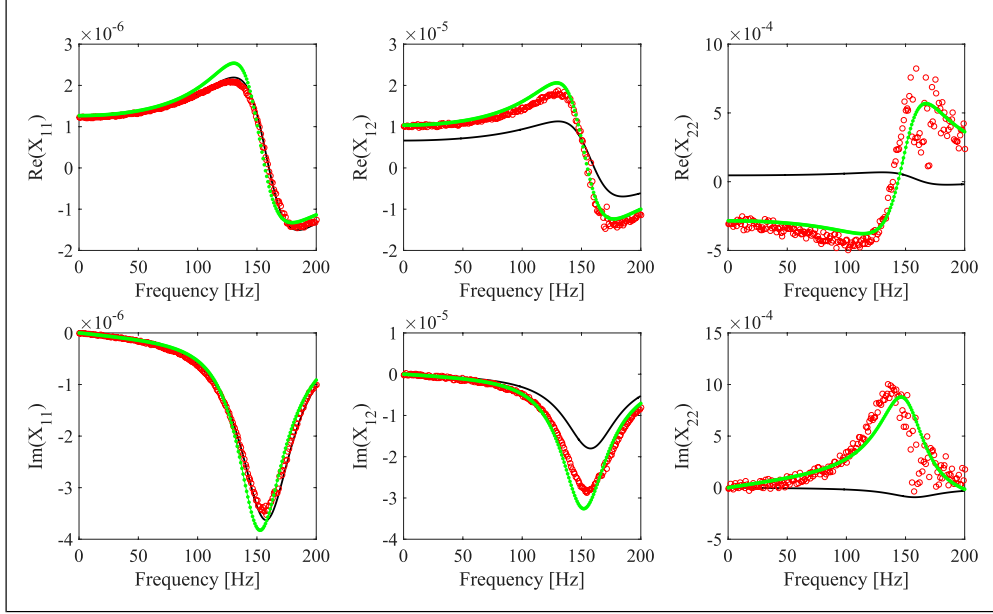


Figure 5. $\bar{\mathbf{X}}(\omega)$ reference model (black); $\mathbf{X}(\omega)$ estimated values from virtual measurements with added noise ($S/N = 80$ dB) (red) and rational fit (green).

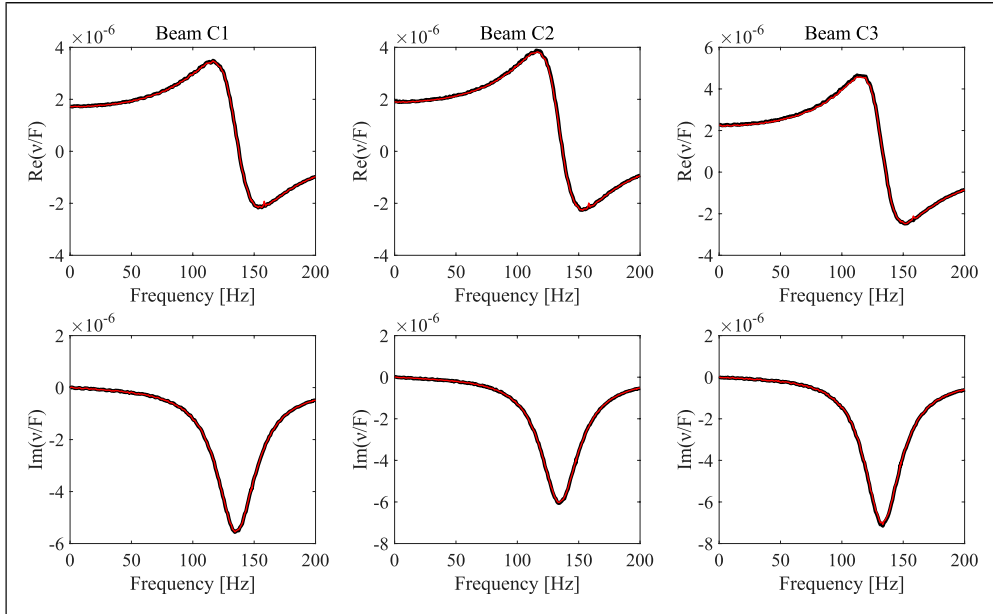


Figure 6. Comparison of measured v/F (black) and estimated v/F using the $\mathbf{X}(\omega)$ rational fit (red) for beam C1, C2 and C3 (Table 2) with added noise ($S/N = 80$ dB).

not taken into account, with respect to $D(\omega)$ plot results and the associated identified SLS parameters. With respect to $S/N = 80$ dB simulated noise measurements identification results, $D(\omega)$ plots show that rational fit identified values closely approximate reference values and the error associated to the identified SLS parameters (Table 2) with respect to reference values (Table 3) is low.

9. Experimental measurements

Some experimental test cases are considered. Measurements are made with a TA Instruments Q800 DMA, single-cantilever experimental setup (Figure 2), in the $[0.1, 200]$ Hz frequency range, $n_f = 202$ and ambient constant temperature (30°C). The maximum applied strain is 0.05%, compatible with the small deformation model assumption. A set of

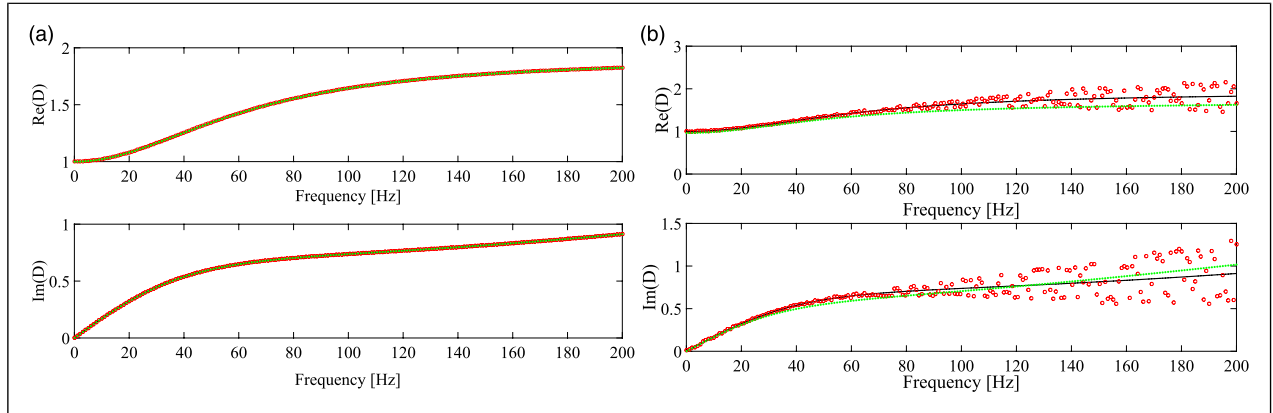


Figure 7 $\bar{D}(\omega)$ reference model (black), $D(\omega)$ estimated values (red) and rational fit (green) from beam D1 (Table 2), virtual measurement without (a) and with (b) added noise ($S/N = 80$ dB).

Table 3. SLS material model from simulated test data.

Specimen	N	E_i [Pa]	β_i [Pa·s]
D1 (no noise)	2	$3.804 \cdot 10^{10}$	$1.9 \cdot 10^8$
		$4.303 \cdot 10^{10}$	$1.101 \cdot 10^7$
D1 ($S/N = 80$ dB)	2	$3.850 \cdot 10^{10}$	$1.998 \cdot 10^8$
		$4.155 \cdot 10^{10}$	$1.204 \cdot 10^7$

Table 4. Experimental test case beam models.

Specimen	Material	L [mm]	Width w [mm]	Thickness t [mm]	ρ [kg/m ³]	E_0 [Pa]
G1	C67 harmonic steel	17.5 ± 0.01	12.7 ± 0.01	0.75 ± 0.01	7850 ± 5	$(2.1 \pm 0.05) \cdot 10^{11}$
G2	C67 harmonic steel	13.05 ± 0.01	12.7 ± 0.01	0.75 ± 0.01	7850 ± 5	$(2.1 \pm 0.05) \cdot 10^{11}$
G3	C67 harmonic steel	9.35 ± 0.01	12.7 ± 0.01	0.75 ± 0.01	7850 ± 5	$(2.1 \pm 0.05) \cdot 10^{11}$
H1	C67 harmonic steel	15.1 ± 0.01	12.7 ± 0.01	0.75 ± 0.01	7850 ± 5	$(2.1 \pm 0.05) \cdot 10^{11}$
H2	Cyanoacrylate polymer/St powder mix	17.5 ± 0.01	4.2 ± 0.01	1.83 ± 0.01	3250 ± 5	$(4.5 \pm 0.1) \cdot 10^9$

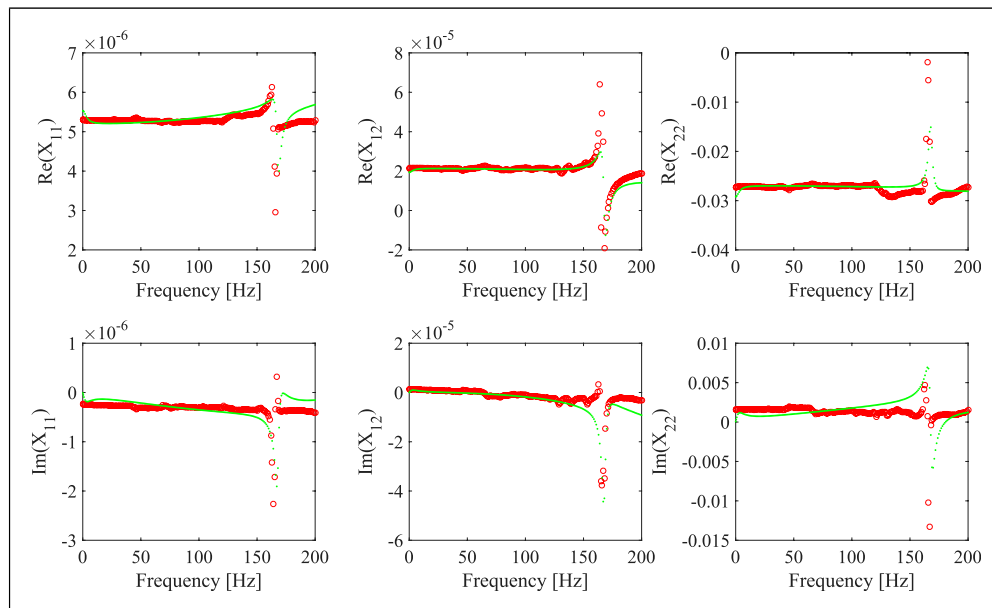


Figure 8. $X_{(1,1)}(\omega)$, $X_{(1,2)}(\omega)$ and $X_{(2,2)}(\omega)$ estimated values from experimental measurements (red) and rational fit (green).

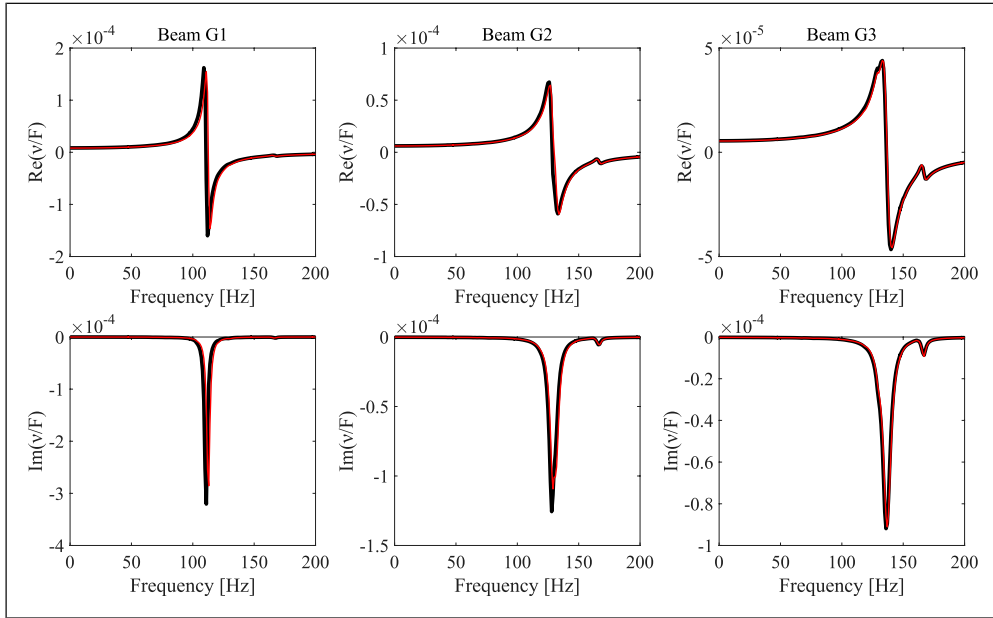


Figure 9. Comparison of measured v/F (black) and estimated v/F using the identified frame rational function (red) for beam G1, G2 and G3 (Table 4).

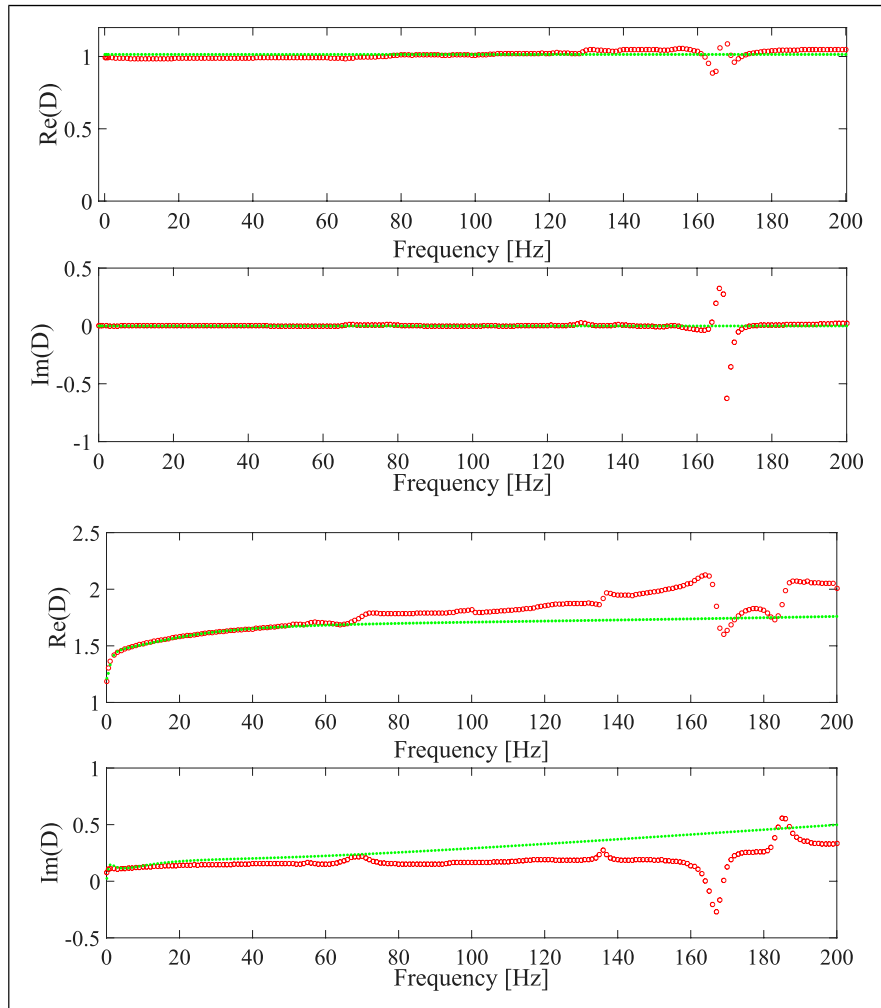


Figure 10. $D(\omega)$ estimated values (red) and rational fit (green) from experimental measurement on HI (a) and H2 (b) specimens.

Table 5. SLS material model from experimental test data.

Specimen	N	E_i [Pa]	β_i [Pa·s]
H1	1	$2.1 \cdot 10^{11}$	0
H2	3	$7.41 \cdot 10^9$	$2.352 \cdot 10^6$
		$3.18 \cdot 10^{10}$	$2.570 \cdot 10^8$
		$1.991 \cdot 10^{10}$	$3.524 \cdot 10^9$

measurements is made on three harmonic steel beam specimens of different geometry (beams G1–G3, Table 4). The instrument frame FRFs, $X_{(1,1)}(\omega)$, $X_{(1,2)}(\omega)$ and $X_{(2,2)}(\omega)$ (Figure 8), are identified by means of the experimental measurements on the G1–G3 test beams.

In order to test the effectiveness of this identification procedure, the $h(\omega)$ measurements related to beams G1–G3 versus the same data obtained from numerical simulation, adopting the identified $\mathbf{X}(\omega)$ model and the beam reference test data reported in Table 4, are shown in Figure 9: it appears that the numerically simulated data are practically coincident with the experimental test data. Experimental measurements on new test beams (H1–H2, Table 4) are made and the specimen $D(\omega)$ SLS material model is identified as well. Beam H2 is prepared by mixing a commercially available modified ethyl cyanoacrylate polymeric material (Loxal instant 47 gel[®], 0.66 volume ratio) and an environmentally sustainable steel powder obtained from recycled machining waste chip (10 mm mean grain size, 0.33 volume ratio).

Results are reported in Figure 10 and Table 5. The results concerning the material rational fit model of H1 specimen show to be effective and coherent with the expected values since a $N = 1$ block SLS model is identified from the C67 steel, $D(\omega) = 1$, while the results concerning the material rational fit model of specimen H2 are associated to a physically sound $N = 3$ blocks SLS model. The H1 identification results appear to be coherent and consistent with the material under study, since as expected no material poles in the Δ frequency range were found, so that a Hooke material model results. Three stable poles resulted from SLS parameter identification related to unknown H2 material specimen. The difference from identified rational $D(\omega)$ plots with respect to estimated plots can be attributed to experimental noise, since such error could only be minimized by taking into account the unphysical complex poles, being not consistent with the assumed SLS model.

10. Conclusions

A procedure for the identification of the material standard linear solid model parameters by means of dynamical measurements is presented. The real E_i and β_i SLS parameters are identified by means of an algebraic technique dealing with the experimental estimate of the reciprocal of $D(\omega)$ expressed as a ratio of polynomial functions. Taking into account the

only physically sound real E_i and β_i parameters, a stability procedure is also introduced to estimate the optimal order of the material SLS model. It must be outlined that such model approach makes it also possible to extrapolate the material behaviour outside the Δ measurement frequency range.

The proposed technique is effective because the contribution of the instrument frame and of the specimen and measurement subsystem inertia are fully taken into account in the whole measurement frequency domain. Numerical simulations taking into account the contribution of noise showed that the proposed numerical procedure is robust enough with respect to the SLS material model identification task. Since the technique only takes into account the I/O measurements made by the force and displacement sensors available in a standard DMA system, it can be successfully applied in most commercially available system contexts.

The accuracy of the procedure aiming to identify the frame contribution was found to strongly depend on the correct choice of the set of the test reference specimens used to identify the instrument frame, strictly depending on the specific instrument frame architecture, the frequency resolution available in the test frequency range and on the measurement digital accuracy associated to the DMA sensors. Nevertheless, a procedure based on the Svd algebraic algorithm was outlined in Section 4, equation (22), to help the experimentalist to choose the optimal set of the reference specimens.

It should be outlined that the identification of such optimal set of test reference specimens can be time consuming but it theoretically needs to be made only once with respect to each test setup.

The application of this approach showed to be effective in all of the test cases approached in this work.

Future work will be addressed towards the identification of non-standard SLS material models, such as models employing hysteretic and fractional derivative based dissipative components, and to the identification of the material model of the coating layers employed in a multilayer architecture.

Acknowledgements

This study was developed within the CIRI-MAM with the Regione Emilia Romagna, POR Fesr Tecnopoli project. Technical support from Andrea Zucchini, Danilo Persici from Marzocchi Pompe S.p.A., Casalecchio di Reno, Italy, and from Massimo Penatti and Alessandra Maino from Loxal s.r.l. is also kindly acknowledged.

Declaration of conflicting interests

The author(s) declared no potential conflicts of interest with respect to the research, authorship, and/or publication of this article.

Funding

The author(s) received no financial support for the research, authorship, and/or publication of this article.

ORCID iD

Stefano Amadori  <https://orcid.org/0000-0002-3200-2460>

References

- Allemang RJ and Phillips AW (2004) The unified, matrix polynomial approach to understanding modal parameter estimation: an update. In: Proceedings of the 2004 international conference on noise and vibration engineering, (ISMA 2004), Leuven, Belgium, September 2004.
- Amadori S and Catania G (2016) Experimental identification of the constitutive model of viscoelastic non-standard materials. In: Proceedings of ASME international mechanical engineering congress and exposition, volume 13 (Code 128056) (IMECE 2016), Phoenix, United States, 11 November 2016.
- Amadori S and Catania G (2017) Robust identification of the mechanical properties of viscoelastic non-standard materials by means of frequency domain experimental measurements. *Composite Structures* 169: 79–89.
- Amadori S and Catania G (2021) Material model robust identification procedure from dynamical measurements made on a flexible specimen-frame system. *Composite Structures* 269. DOI: [10.1016/j.compstruct.2021.113981](https://doi.org/10.1016/j.compstruct.2021.113981).
- ASTM International (2015a) *Standard Test Method for Plastics: Dynamic Mechanical Properties: In Flexure (Three-Point Bending)*. West Conshohocken, PA: ASTM International, (Publication No D5023-07).
- ASTM International (2015b) *Standard Test Method for Plastics: Dynamic Mechanical Properties: In Flexure (Dual Cantilever Beam)*. West Conshohocken, PA: ASTM International, (Publication No D5418-15).
- Bogatyrev AB (2010) Chebyshev representation for rational function. *Sb. Math* 201: 1579–1598.
- Cacioppoli R (1930) Un teorema generale sull'esistenza di elementi uniti in una trasformazione funzionale. *Rend. Acc. Naz. Lincei* 6(11): 794–799.
- Danley RL (2018) Dynamic mechanical analyzer and sample fixture for dynamic mechanical analyzer. US patent 9,933, 249.
- Dankovi B, Antic D, Jovanovic Z, et al. (2009) Systems modeling based on legendre polynomials. In: 5th international symposium on applied computational intelligence and informatics, Timisoara, Romania, 28–29 May 2009.
- Ehrenstein GW, Trawiel P and Riedel G (2004) *Thermal Analysis of Plastics Theory and Practice*. München, Germany: Carl Hanser Verlag GmbH & Co. KG.
- Ewins DJ (2000) *Modal Testing: Theory, Practice and Applications*. 2nd edition. Hertfordshire: Research Studies Press Ltd.
- Findley WN, Lai JS and Onaran K (1989) *Creep and Relaxation of Nonlinear Viscoelastic Materials*. New York: Dover publications Inc.
- Forsythe GE (1957) Generation and use of orthogonal polynomials for data-fitting with a digital computer. *Journal of the Society of Industrial Applied Mathematics* 5(2): 74–85.
- Forsythe GE, Malcolm MA and Moler CB (1977) *Computer Methods for Mathematical Computations*. Englewood Cliffs, NJ: Prentice-Hall.
- Giuliani P, Di Maio D, Schwingshackl CW, et al. (2013) Six degrees of freedom measurement with continuous scanning laser doppler vibrometer. *Mechanical Systems and Signal Processing* 38(2): 367–383.
- Granas A and Dugundji J (2003) *Fixed Point Theory*. New York: Springer-Verlag.
- Huynh HN, Assadi H, Dambly V, et al. (2021) Direct method for updating flexible multibody systems applied to a milling robot. *Robotics and Computer-Integrated Manufacturing* 68: 102049.
- Huynh HN, Assadi H, Lorphèvre ER, et al. (2020) Modelling the dynamics of industrial robots for milling operations. *Robotics and Computer-Integrated Manufacturing* 61: 101852.
- Kelly LG (1967) *Handbook of Numerical Methods and Applications*. Boston, Massachusetts: Addison Wesley Publishing Company.
- Kostka P, Holeczek K, Hohne R, et al. (2016) Extension and application of dynamic mechanical analysis for the estimation of spatial distribution of material properties. *Polymer Testing* 52: 184–191.
- Liu B, Xu J and Li Y (2014) Constitutive investigation on viscoelasticity of Polyvinyl butyral: experiments based on dynamic mechanical analysis method. *Advances in Materials Science and Engineering* 2014: 794568.
- McAninch IM, Palmese GR, Lenhart JL, et al. (2015) DMA testing of epoxy resins: the importance of dimensions. *Polymer Engineering and Science* 55: 2761–2774.
- Menard KP (2008) *Dynamic Mechanical Analysis: A Practical Introduction*. 2nd edition. Boca Raton, Florida: CRC Press.
- Oregui M, Man AD, Woldekidan MF, et al. (2016) Obtaining railpad properties via dynamic mechanical analysis. *Journal of Sound and Vibration* 363: 460–472.
- Peumans D, De Vestel A, Busschots C, et al. (2019) Accurate estimation of the non-parametric FRF of lightly-damped mechanical systems using arbitrary excitations. *Mechanical Systems and Signal Processing* 130: 545–564.
- Phillips AW, Allemang RJ and Brown DL (2011) Autonomous modal parameter estimation: methodology. In: Conference proceedings of the society for experimental mechanics series (eds T Proulx) *Modal Analysis Topics Volume 3*. New York, NY: Springer.
- Placet V and Foltete E (2010) Is Dynamic Mechanical Analysis (DMA) a non-resonance technique? the European physical journal conferences volume 6. In: Proceedings of the 14th international conference on experimental mechanics (ICEM 14), Boca Raton, Florida, June 2010 (article number 41004).
- Read BE and Dean GD (1978) *The Determination of Dynamic Properties of Polymers and Composites*. Bristol, England: Adam Hilger Ltd.
- Richardson MH and Formenti DL (1982) Parameter estimation from frequency response measurements using rational fraction polynomials. In: Proceedings of 1st IMAC conference, Orlando, FL, November 1982.
- Schalnat J, Garoz Gómez D, Daelemans L, et al. (2020) Influencing parameters on measurement accuracy in dynamic mechanical analysis of thermoplastic polymers and their composites. *Polymer Testing* 91: 106799. DOI: [10.1016/j.polymertesting.2020.106799](https://doi.org/10.1016/j.polymertesting.2020.106799).
- Shilov GE (1996) *Elementary Real and Complex Analysis*. New York: Dover.

- Stanbridge AB and Ewins DJ (1999) Modal testing using a scanning laser doppler vibrometer. *Mechanical Systems and Signal Processing* 13(2): 255–270.
- Storage T, Brockman R and Tienda KM (2013) *Analysis of Data Reduction Strategy Used in TA Instruments Q800 DMA Test System*. Available at: <https://apps.dtic.mil/dtic/tr/fulltext/u2/a591605.pdf>.
- Swaminathan G and Shivakumar K (2009) A re-examination of DMA testing of polymer matrix composites. *Journal of Reinforced Plastics and Composites* 28(8): 979–994. DOI: 10.1177/0731684407087740.
- Timoshenko S, Young DH and Weaver W (1974) *Vibration Problems in Engineering*. Hoboken, NJ: John Wiley & Sons.
- Warren C, Niezrecki C, Avitabile P, et al. (2011) Comparison of FRF measurements and mode shapes determined using optically image based, laser, and accelerometer measurements. *Mechanical Systems and Signal Processing* 25(6): 2191–2202.
- Xu X and Gupta N (2018) Determining elastic modulus from dynamic mechanical analysis data: reduction in experiments using adaptive surrogate modeling based transform. *Polymer* 157: 166–171.